INSTITUTE OF PHYSICS PUBLISHING JOURNAL OF PHYSICS: CONDENSED MATTER

J. Phys.: Condens. Matter **18** (2006) 10751–10763 doi:10.1088/0953-8984/18/48/003

Adsorption of methanol and methoxy on the α-Cr_2O_3(0001) surface

Øyvind Borck[1,2] **and Elsebeth Schröder**[2]

[1] Department of Physics, Norwegian University of Science and Technology, NO-7034 Trondheim, Norway
[2] Department of Applied Physics, Chalmers University of Technology, SE-41296 Göteborg, Sweden

E-mail: oyvind.borck@ntnu.no

Received 18 June 2006, in final form 2 October 2006
Published 17 November 2006
Online at stacks.iop.org/JPhysCM/18/10751

Abstract

We present density functional theory calculations of methanol and methoxy adsorption at the Cr-terminated α-Cr_2O_3(0001) surface. We report on the equilibrium geometries of the adsorbed methanol and methoxy molecules, analyse the bonding to the surface, and discuss the dissociation energetics of methanol into methoxy on the surface. We found that methanol adsorbs with its O atom situated above a threefold coordinated hollow site in the surface O layer at a distance of 2.12 Å from the nearest-neighbour Cr atom, and with a calculated adsorption energy of 0.82 eV. For the methoxy molecule we found the optimum adsorption geometry to be with the methoxy O on top of a Cr atom and with the CO-axis tilted away from the surface normal by ∼55°. Methoxy is strongly bound to the surface with an estimated adsorption energy of 3.3 eV.

(Some figures in this article are in colour only in the electronic version)

1. Introduction

The chromium oxides find a wide variety of uses in technological applications, as catalysts (polymerization of ethylene [1, 2], dehydrogenation [3], NO_x reduction [4], etc), gas sensors [5], protective layer [6, 7] (corrosion resistance promotion, wear resistance, stainless steel passivation layer), adhesion promoter [7, 8], and magnetic recording media [9]. The aluminium in construction materials is aluminium alloys, whose surfaces are often treated by a chromate conversion coating (CCC) process [8]. The CCC improves the corrosive resistance and adhesive properties of the surface [7, 8]. The coating can be applied by spraying, or by dipping the aluminium product in an aqueous acidic solution containing chromium salts [8]. The precise composition of the coating that results from this treatment depends on several factors, including the preceding surface preparation, the composition of the bath, and the

presence of intermetallic particles in the substrate, though it is known that Cr_2O_3 is a major constituent of the outermost part of the coating. Unfortunately, the hexavalent chromium found in the solution presents severe health and environmental concerns. For this reason, considerable work has been put into developing alternatives to CCC, but so far few surface pretreatments have been able to match the performance of CCC [10].

Searching for alternatives to CCC, a detailed knowledge of how the CCC improves adhesion would be helpful. At a fundamental level, adhesion results from the interaction of organic polymers, e.g., epoxy resins, of the paint or adhesive with the substrate surface. The complexity of polymer–surface interactions is such that the full polymer interaction cannot be fully described on an atomic length scale. One strategy is thus to focus on how fragments of the polymer—single functional groups—interact with the surface, focusing on those fragments known or expected to have the largest influence on the adhesion of the full polymer. In this study methanol and methoxy are chosen as representative molecules. We use the α-$Cr_2O_3(0001)$ surface to represent the CCC. Although this surface is admittedly very simplified compared to the industrial CCC surface, we believe it provides a good starting point for understanding the physics and chemistry of the CCC. The (0001) surface of α-Cr_2O_3 has been subject to various theoretical and experimental studies in recent years, investigating the properties of the clean surface [11–16], and the interaction of small molecules, such as H_2O [17, 18], CO [19], CO_2 [20], and ethene [21], with the surface.

Theoretical studies of organic molecules on ionic crystal surfaces are largely lacking in the literature. We have previously [22, 23] studied the adsorption of methanol on α-$Al_2O_3(0001)$, a surface which is isostructural to α-$Cr_2O_3(0001)$, and found that the adsorption bond there is relatively strong with a pronounced donor–acceptor character in the sense that one of the atoms (methanol O) contributes electron charge to create the binding of methanol O in the stable site on top of a surface Al ion. In the present work we report on density functional theory (DFT) calculations of molecular adsorption of methanol (CH_3OH) at the α-$Cr_2O_3(0001)$ surface. Methanol is the smallest member of the alcohols and adsorption of methanol on α-$Cr_2O_3(0001)$ represents a prototype for understanding the interaction of hydroxyl (OH) groups in alcohols and some biological molecules with flexible oxide surfaces. Targets for our study are adsorption site and strength, the nature of the adsorption bond, and other characteristics of the adsorbate. It is not uncommon for the hydroxyl group to loose its hydrogen atom in a reaction with the surface; we therefore also report on the adsorption of methoxy (CH_3O) on this surface and evaluate the energy gain of the methanol-to-methoxy dissociation. Furthermore, it is of interest to contrast the interaction of the closed-shell methanol molecule and open-shell methoxy molecule with the α-$Cr_2O_3(0001)$ surface.

The paper is organized as follows. A brief account of our computational method is given in section 2. In section 3 we present results for bulk α-Cr_2O_3 and the clean (0001) surface. Section 4 contains our results for the adsorption geometries and energies for methanol and methoxy at 1 ML and 1/4 ML and we discuss the nature of bonding between the adsorbates and the substrate. The paper is concluded with a short discussion and concluding remarks in section 5.

2. Computational method

The DFT calculations presented here were conducted using the plane-wave pseudo-potential code DACAPO [24]. We employed ultrasoft pseudo-potentials [25] and the generalized gradient approximation (GGA) in the PW91 parameterization [26]. In all calculations, spin-polarization is allowed for. The energy cut-off for the plane-wave expansion is 400 eV, and the irreducible Brillouin zone is sampled using the Monkhorst–Pack scheme [27].

The α-Cr_2O_3(0001) surface is represented by a slab periodically repeated in all directions, consisting of a finite number of layers of Cr–O_3–Cr that are separated by a vacuum gap. For most of the calculations on the methanol and methoxy adsorption, a slab of four layers separated by a vacuum gap of width 15 Å is used, with a (1×1) superstructure containing one molecule per surface unit cell. Defining coverage with respect to the surface Cr layer, we will refer to this coverage as $\Theta = 1$ ML. Molecules are placed on one side of the slab only, and the artificial electric field created by the asymmetry of the system is compensated by a self-consistently determined dipole correction applied in the vacuum region [28, 29].

The equilibrium structures are found by locally minimizing the Hellmann–Feynman forces until the remaining total force on the unconstrained atoms is less than 0.05 eV $Å^{-1}$. A preconditioned quasi-Newton method based on the Broyden–Fletcher–Goldfarb–Shanno algorithm [30] is used for the structure optimization. During structure optimizations, the atoms of the bottom Cr–O_3–Cr layer of the slab are kept fixed in the bulk geometry. All other atoms are allowed to relax freely; no symmetry constraints are applied. For the (1×1) surface unit cell we use a $4 \times 4 \times 1$ k-point mesh. The geometries of isolated (gas-phase) methanol and methoxy are optimized in fcc cells of side length 14 Å in which only the Γ-point of the Brillouin zone is sampled.

To investigate the coverage dependence of the methanol and methoxy adsorption, additional calculations were carried out using a (2×2) surface unit cell corresponding to $\Theta = 1/4$ ML. Tests with larger vacuum and slab thickness, higher cut-off energy and denser k-point sampling show negligible changes in the energies and structural parameters, as described and discussed in section 4.

The heat of formation per formula unit for the α-Cr_2O_3 bulk, ΔH_f^0, is calculated using

$$\Delta H_f^0 = -(E_{Cr_2O_3}^{bulk} - 2E_{Cr}^{bulk} - (3/2)E_{O_2}) \tag{1}$$

where $E_{Cr_2O_3}^{bulk}$, E_{Cr}^{bulk}, and E_{O_2} are the total energies of bulk α-Cr_2O_3, of bulk Cr, and of the gas phase oxygen molecule. The adsorption energy per molecule is calculated from

$$E_{ads} = -(E_{SM} - E_S - E_M), \tag{2}$$

where E_{SM} is the total energy of the α-Cr_2O_3 slab with adsorbed methanol (or methoxy), E_S is the energy of a clean slab of α-Cr_2O_3, and E_M is the energy of an isolated methanol (or methoxy) molecule. With this definition, a positive energy indicates that the adsorption is exothermic (stable).

To calculate local properties like atomic charge (ionicity) and the magnetic moment of the individual atoms and to quantify charge transfer we used Bader's 'Atoms-in-Molecules' (AIM) method [31]. Here the electron density is divided into atomic regions Ω, or basins, enclosed by surfaces defined by

$$\nabla n(\mathbf{r}) \cdot \mathbf{l} = 0, \tag{3}$$

where $\mathbf{l}$ is the unit vector normal to the surface. Atomic properties are obtained by integrating over the individual basins, e.g., the charge of an atom A enclosed within basin Ω_A is obtained by integrating the electron density over Ω_A and subtracting the obtained value from the charge of the isolated atom:

$$Q_A = Z_A - \int_{\Omega_A} d\mathbf{r}\, n(\mathbf{r}). \tag{4}$$

Similarly, the magnetic moment is calculated by integrating the difference between the spin-up and spin-down electron density over the atomic basin,

$$m_A = \int_{\Omega_A} d\mathbf{r}\, [n_\uparrow(\mathbf{r}) - n_\downarrow(\mathbf{r})]. \tag{5}$$

Table 1. Bulk properties of α-Cr_2O_3. The lattice constants a and c of the hexagonal unit cell, the short and long Cr–O distances d_{CrO1} and d_{CrO2}, the bulk modulus B_0, and the heat of formation ΔH_f^0.

	a (Å)	c (Å)	d_{CrO1} (Å)	d_{CrO2} (Å)	B_0 (GPa)	ΔH_f^0 (eV/Cr_2O_3)
Calc.	4.96	13.81	1.98	2.02	209	10.41
Expt.	4.951[a]	13.566[a]	1.962[a]	2.009[a]	238[a], 231[b]	11.76[c]

[a] Reference [35].
[b] Reference [36].
[c] Reference [37].

We used the algorithm described in [32] to decompose the electron density into Bader's atomic basins. In this scheme the accuracy of the results can be systematically improved by decreasing the grid-point separation of the fast Fourier transform (FFT) grid used to represent the electron density. We used a gridpoint separation of 0.08 Å. Test calculations indicated that this choice will result in errors of the order of 0.01 $|e|$.

3. Bulk α-Cr_2O_3 and clean α-Cr_2O_3(0001)

Bulk α-Cr_2O_3, like α-Al_2O_3, crystallizes in a rhombohedral structure with the space group D_{3d}^6 ($R\bar{3}c$), and the primitive unit cell contains two formula units [33]. The crystal structure can alternatively be described as a hexagonal close-packed array of oxygens, in which the Cr atoms occupy 2/3 of the interstitial octahedral sites. The Cr layer is slightly rumpled, resulting in two distinct interatomic Cr–O distances. Below the Néel temperature $T_N \sim 310$ K [34], α-Cr_2O_3 is an antiferromagnetic insulator with the spin sequence $+-+-$ along the threefold axis.

Table 1 lists calculated and experimental bulk structural properties for α-Cr_2O_3. The optimized geometry and bulk modulus have been obtained following the procedure proposed in [38]. The calculated bulk properties listed in table 1 compare well with the experimental values, and with other GGA calculations [16, 39]. The slight overestimate of the structural parameters and underestimate of the bulk modulus is a well known feature of the GGA [40–42]. We found that the antiferromagnetic spin-ordering yields a ground-state energy that is lower than the ferromagnetic and paramagnetic phase equilibrium energies by 0.2 and 1.6 eV per formula unit, respectively. In the antiferromagnetic spin-ordering we calculated the magnetic moment per Cr atom $m_{Cr} = 2.66\,\mu_B$, a result that should be compared to the experimental values 2.76 μ_B [34] and 2.48 μ_B [43]. We found no net magnetic moment on the O atoms.

The atomic charge can be calculated by integrating the charge density over the Bader atomic basins. Doing this we find charges $Q_{Cr} = +1.73\,|e|$ and $Q_O = -1.15\,|e|$ respectively. The deviation from the formal ionicity (+3 and −2) may be interpreted as due to a covalent contribution to the bonding in α-Cr_2O_3. In comparison, in α-Al_2O_3 the charges $Q_{Al} = +2.50\,|e|$ and $Q_O = -1.67\,|e|$ are closer to the formal ionicity, the bonds in α-Al_2O_3 having more of an ionic character than in α-Cr_2O_3.

Figure 1 shows the density of states projected (PDOS) onto the Cr 3d and O 2p states. The O and Cr s states and Cr 3p states have no significant weight in the energy range shown. The valence band structure compares well to spectroscopic data [44]. The upper part of the valence band consists mainly of Cr 3d-derived states separated from a broad band of mainly O 2p character. Note however that there is a significant hybridization of Cr 3d and O 2p states over the whole valence band region. The calculated band gap is $E_g = 1.7$ eV, which is 47% smaller than the experimental value $E_g = 3.2$ eV determined from combined photoemission and inverse photoemission spectra [44].

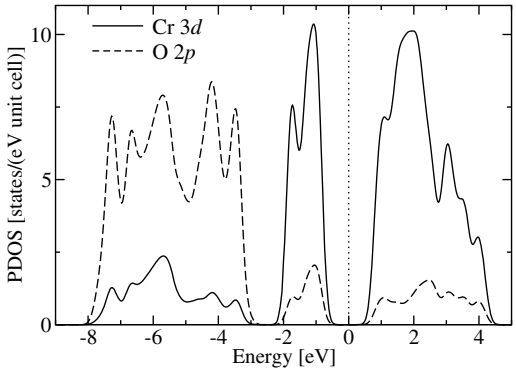

Figure 1. Projected density of states (PDOS) for bulk Cr_2O_3. The density of states has been projected onto the 3d state of Cr and 2p state of O. The PDOS for the spin-up and spin-down components are identical (because α-Cr_2O_3 is an antiferromagnet); here we plot the PDOS for the sum over both spins. The Fermi energy as calculated by DACAPO is used as the reference energy.

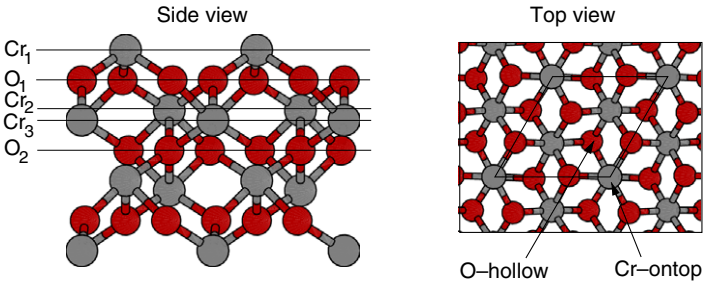

Figure 2. Schematic side and top view of the α-Cr_2O_3(0001) surface terminated by chromium. The left panel shows the three-layer slab. O (Cr) atoms are shown as dark (light) circles. The sites indicated are discussed in the text.

Along the trigonal [0001]-axis of α-Cr_2O_3, layers of oxygen alternate with two metal layers in the stacking sequence $\cdots$Cr–Cr–O_3–Cr–Cr–$O_3\cdots$. The (0001) surface can be obtained by cleaving the crystal in between any of these layers; hence there are three chemically different terminations. Low-energy electron diffraction (LEED) [12] and scanning transmission microscopy (STM) [13] experiments indicate that under ultrahigh-vacuum (UHV) conditions the α-Cr_2O_3(0001) surface is terminated by a single layer of Cr. Theoretical work has shown that depending on temperature and oxygen partial pressure, the surface may be oxygen or chromyl (Cr=O) terminated [15, 16]. In the present work we consider the chromium-terminated surface, which corresponds to the surface observed under UHV conditions (figure 2).

Similar to other corundum-type oxides (α-Al_2O_3 and α-Fe_2O_3), α-Cr_2O_3(0001) shows a significant relaxation of the surface layers compared to the ideal bulk termination. Table 2 gives an overview of our relaxation data compared to previous theoretical works and a LEED experiment by Rohr *et al* [12]. The theoretical results are in qualitative agreement with each other and are—with the exception of the second atomic layer where we predict an expansion rather than a contraction—in good agreement with the experimental data, showing a strong relaxation of the surface compared to the bulk-truncated surface.

Table 2. Relaxations of the outermost atomic layers of the α-$Cr_2O_3(0001)$ surface given in percentage of bulk interlayer separations.

		Previous theoretical works					Experiment
	This work GGA	HF[a] [11]	MD simul.[b] [12]	FP-LAPW[c] [14]	GGA [16]	GGA + U[d] [16]	LEED [12]
Cr_1–O_1	−60.9	−49.8	−58	−59	−62	−60	−60
O_1–Cr_2	+4.4	+3.3	0	+1	+10	+12	−3
Cr_2–Cr_3	−36.5	—	−36	−38	−41	−44	−21
Cr_3–O_2	+5.6	—	+17	+10	+6.5	+9.2	+6

[a] HF: Hartree–Fock approximation.
[b] MD simul.: molecular dynamics simulation.
[c] FP-LAPW: full-potential linear augmented plane-wave method.
[d] GGA + U: generalized gradient approximation including on-site Coulomb interactions.

4. Adsorption of methanol and methoxy

The key properties of the adsorption are the preferred adsorption site, the orientation of the adsorbed molecule with respect to the surface, the adsorption energy, and the change in electronic structure upon adsorption.

4.1. Adsorption geometry and energetics

To determine the optimum adsorption structure for methanol and methoxy on α-$Cr_2O_3(0001)$ we performed a series of structure optimizations with the adsorbate initially placed with its O atom on top of one of the five different high-symmetry sites on exposed atoms of the surface. We also considered various starting orientations of the molecules with respect to the surface. During the optimizations, no motional constraints are placed on the atoms of the adsorbates or the slab, with the exception of the bottom Cr–O_3–Cr layer, which is kept fixed in the bulk-truncated geometry. The molecules are therefore allowed to move freely on the surface and to change their orientation to locate the minimum energy structure. From this set of calculations, we found that all candidate structures optimize to only one adsorption structure for methanol (site 'O-hollow' in figure 2) and one for methoxy (site 'Cr-ontop' in figure 2), independent of the starting site and initial orientation. These adsorption optimum structures are shown schematically in figures 3 and 4, and table 3 summarizes the adsorption energies and geometric data.

Convergence tests. We explored the influence of the number of slab layers on the results by using slabs of three, four and five Cr–O_3–Cr layers, where in each case the bottom layer is kept fixed in the bulk-truncated geometry. The results for the three- and four-layer slab, summarized in table 3, show only small differences in the adsorption geometry, the difference in adsorption energy being 0.02–0.04 eV. The adsorption energy using a five-layer slab differs by less than 0.01 eV compared to the four-layer slab, and the changes in adsorption geometry are negligible. The four-layer slab is therefore sufficient to describe the adsorption of methanol and methoxy, and even the three-layer slab gives adequate results.

To investigate the influence of coverage we did additional calculations with one adsorbate per (2×2) surface unit cell, i.e., at coverage $\Theta = 1/4$ ML. For these calculations we used a three-layer slab and a $2 \times 2 \times 1$ Monkhorst–Pack mesh. As can be seen from table 3, there are only small or no changes in the adsorption energies and geometries at coverage $\Theta = 1/4$ ML compared to coverage $\Theta = 1$ ML.

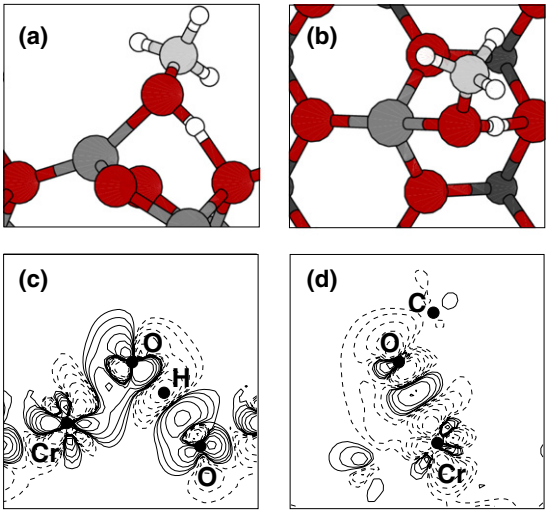

Figure 3. Schematic side view, (a), and top view, (b), of the optimum adsorption geometry for methanol on Cr_2O_3(0001) found in our calculation. Panels (c) and (d) show contour plots of the valence electron density difference, $\Delta n(\mathbf{r})$. Panel (c) displays a cross section containing one surface Cr and O atom, and the methanol O and H atoms, where the H atom is the one belonging to the methanol OH group. In panel (d), the cross section passes through the C and O atoms of methanol and the surface layer Cr atom. Solid (dashed) lines indicate gain (loss) of electron density. The contours are drawn at densities $\Delta n = \pm 0.005 \times 2^k\ e/\text{Å}^3$ for $k = 0, 1, 2, 3, 4, 5$.

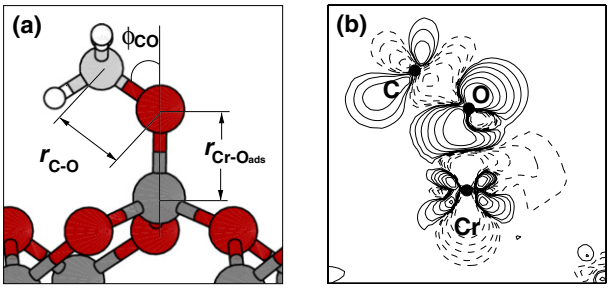

Figure 4. (a) Schematic side view of the optimum adsorption structure for methoxy on Cr_2O_3(0001). (b) Contour plot of the electron density difference in a cross section containing one Cr and the methoxy O and C atoms. Solid (dashed) lines indicate gain (loss) of electron density. The contours are drawn at densities $\Delta n = \pm 0.005 \times 2^k\ e/\text{Å}^3$ for $k = 0, 1, 2, 3, 4, 5$.

To test whether the use of a fixed bottom layer influences the adsorption energies and geometries we also carried out a test in which all atoms of the slab and adsorbate were allowed to relax. We found no significant changes to the adsorption geometry, and a change in adsorption energy of less than 0.01 eV, thus validating our use of a slab with fixed bottom layer.

We found that the total energy of the isolated molecules, calculated in the side-length 14 Å fcc unit cell with 1 k-point, differs only 0.003 eV from a similar total energy calculation in a 9.91 Å × 9.91 Å × 21.58 Å hcp unit cell with a 2 × 2 × 1 k-point mesh (corresponding to $\Theta = 1/4$ ML without the slab). Further, increasing the plane-wave cut-off from 400 to 450 eV yields a total-energy difference of 0.02 eV. Thus our total energy of the isolated molecules is well converged and does not contribute any significant error to the adsorption energies.

Table 3. Calculated adsorption energy and selected geometrical data for adsorption of methanol and methoxy on α-Cr_2O_3(0001). The distance $r_{Cr-O_{ads}}$ is the distance between the O of the adsorbate and the nearest Cr atom (nearest Al atom), r_{H-O_s} is the shortest distance between H of the molecule hydroxyl group and an O atom at the surface, and h is the vertical spacing between the Cr top layer and the underlying O plane.

	Θ (ML)	Layers	E_{ads} (eV)	h (Å)	$r_{Cr-O_{ads}}$ (Å)	r_{H-O_s} (Å)	r_{O-H} (Å)	r_{C-O} (Å)	$\angle$COH (deg)	ϕ_{CO} (deg)
CH_3OH	Free			0.40			0.98	1.43	109	
	1/4	3	0.80	0.60	2.12	1.59	1.03	1.44	108	53
	1	3	0.80	0.59	2.12	1.52	1.05	1.43	109	52
	1	4	0.82	0.61	2.12	1.54	1.05	1.44	109	52
CH_3O	Free			0.40				1.36		
	1/4	3	3.25	0.62	1.77			1.42		55
	1	3	3.28	0.64	1.77			1.43		55
	1	4	3.32	0.66	1.77			1.43		55
CH_3OH	Free			0.13			0.98	1.43	109	
on	1/4	4	1.23	0.43	1.93	2.03	1.00	1.45	110	57
α-Al_2O_3 [23]	1	4	1.03	0.32	2.00	1.77	1.02	1.44	111	57

We also investigated the influence of k-point sampling and plane-wave cut-off energy, and found the $4 \times 4 \times 1$ Monkhorst–Pack mesh and plane-wave cut-off of 400 eV to be sufficient in the slab and adsorption calculations. Using a $6 \times 6 \times 1$ Monkhorst–Pack mesh or 450 eV cut-off yields essentially the same adsorption energies (differing by less than 0.01 eV) and geometries.

Finally, a test of the vacuum gap size gave converged adsorption energies for a gap equivalent to three slab layers, or 6.9 Å; however, for the structure optimizations a more cautious size of ∼15 Å was used.

Here below we give a more detailed description of the calculated optimum adsorption structures for methanol and methoxy.

Methanol. We found that methanol adsorbs with the O atom situated in the site termed 'O-hollow' in figure 2, independently of our initial positioning of the molecule before structural relaxations. This adsorption site differs from the site found for methanol adsorption on α-Al_2O_3(0001) in our previous results [22, 23]: there the methanol O atom adsorbed nearly on top of an Al atom. In fact, we found that a methanol molecule placed on top of a Cr atom in chromia is strongly repelled by the surface. Comparing also the adsorption energies E_{ads} (table 3) we found that the 0.80–0.82 eV adsorption energy on α-Cr_2O_3(0001), almost unchanged with coverage, is smaller by 0.2–0.4 eV than what we found for adsorption on alumina, on which there is a stronger coverage-dependence.

The methanol molecule on chromia is oriented with the methyl (CH_3) group pointing out from the surface, while the hydroxyl group (OH) points towards a surface layer O (figure 3). The CO-axis is tilted away (by the angle ϕ_{CO}) from the surface normal, slightly less than on alumina, and the molecular dipole plane (the COH plane) is tilted by $\phi_{COH} = 54°$ with respect to the surface plane. In contrast to adsorption on alumina with rather large changes to the surface upon adsorption, the only significant change to the substrate geometry for chromia is that the surface Cr atom is pulled outward by 0.2 Å. In alumina this change in position is coverage-dependent, from 0.2 Å at 1 ML to 0.3 Å at 1/4 ML. As argued in [23], the coverage dependence in alumina originates mostly from deformations in the surface and less on the direct methanol–methanol interaction, and since the surface deforms less in chromia it is to be

expected that having relatively close methanol molecules, as in coverage 1 ML, does not change the adsorption energetics or structure in chromia relative to a more sparse coverage (1/4 ML).

From an atomic structure point of view methanol adsorbs passively on α-Cr_2O_3. Like on alumina, the geometry of the molecule is almost unchanged from the gas phase molecule, with the exception of an elongation of the O–H bond length r_{O-H} by 0.05–0.07 Å. The nearest-neighbour distance of Cr to methanol-O is $r_{Cr-O_{ads}} = 2.12$ Å, significantly larger than the longest Cr-to-O distance in bulk α-Cr_2O_3 of $d_{CrO2} = 2.02$ Å (table 1).

Methoxy. While methanol is repelled from the position with methanol-O on top of Cr, the same site is energetically preferred for methoxy (figure 2). Methoxy has its CO-axis tilted away from the surface normal by $\phi_{CO} = 55°$.

From a separate calculation in which the CO-axis was constrained to be parallel with the surface normal, we estimated the gain in adsorption energy for the tilted compared to the non-tilted geometry to be 0.31 eV. The azimuthal direction of the tilt, on the other hand, is less important energetically. The energy difference in tilting the CO-axis towards the surface O atom compared to a tilt towards an O bridge site is only 0.02 eV, an indication that there is no clear azimuthal preference.

The adsorption energies are considerably larger than what we found for methanol adsorption, and give evidence of a rather strong substrate–adsorbate interaction. The calculated $Cr–O_{ads}$ bond length is $r_{Cr-O_{ads}} = 1.77$ Å, considerably shorter than the bulk Cr–O bond lengths, and also slightly less than the nearest-neighbour distance of 1.79 Å between surface layer Cr and O at the clean surface. The C–O bond of methoxy is elongated from the calculated gas-phase value $r_{C-O} = 1.36$ Å to 1.42–1.43 Å, indicating a weakening of the internal C–O bond due to an electron redistribution to strengthen the surface–molecule bond.

Dissociation. It is energetically expensive to let methanol in the gas phase dissociate by moving off the hydroxyl H atom to form methoxy. Assuming that the removed hydroxyl H atom will form part of a gas phase H_2 molecule the cost is a substantial 2.42 eV per methanol molecule. However, the fact that the energy gain in adsorption of methoxy (3.32 eV at $\Theta = 1$ ML) is considerably larger than that for methanol (0.82 eV at $\Theta = 1$ ML) makes the dissociation marginally favourable on α-Cr_2O_3(0001). Assuming that the removed hydroxyl H atom will stay in the gas phase[3] H_2 the energy gain by surface dissociation is 0.08 eV per methanol molecule, as calculated from our $\Theta = 1$ ML adsorption results, and slightly less when based on our $\Theta = 1/4$ ML results. Thus, on this zero-temperature, idealized, and defect-free chromia surface, ignoring any possible energy barriers, dissociation of methanol is energetically favoured to molecular methanol adsorption. This is in contrast to results for the α-Al_2O_3(0001) surface, where a strong preference for molecular adsorption of methanol is found under the same idealized conditions [45]: the cost of on-surface dissociation is found to be ∼1.3 eV.

4.2. Electronic structure and bonding

To gain insight into the electronic nature of the bonding of methanol and methoxy to the α-Cr_2O_3(0001) surface, we performed separate calculations of the clean surface and isolated molecule in their adsorption geometries, and from these results calculated the electron density difference $\Delta n(\mathbf{r})$ defined as

$$\Delta n(\mathbf{r}) = n_{SM}(\mathbf{r}) - n_S(\mathbf{r}) - n_M(\mathbf{r}) \tag{6}$$

[3] The energy *cost* of adsorbing H as an isolated atom on α-Cr_2O_3(0001) from gas phase $\frac{1}{2}H_2$ is 0.25 eV.

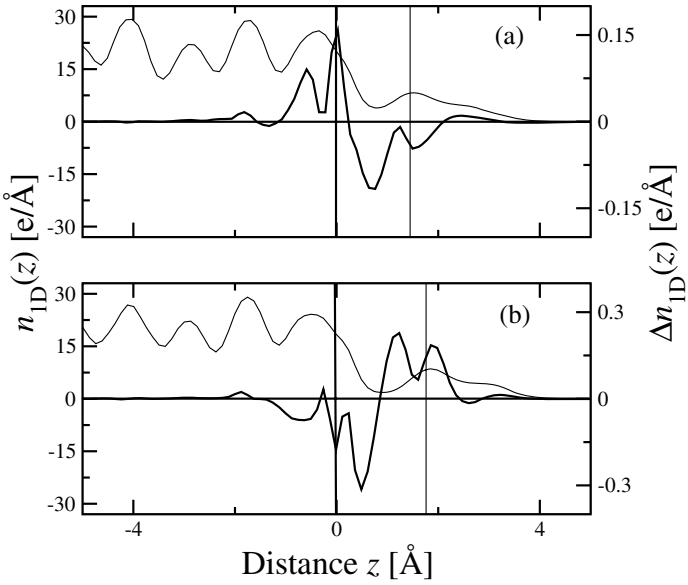

Figure 5. Profile of the total valence electron density, $n_{1D}(z)$, (thin curve) and electron density difference, $\Delta n_{1D}(z)$, (thick curve) at $\Theta = 1$ ML for (a) adsorbed methanol and (b) adsorbed methoxy. The zero-point of the z-axis is set to the position of the topmost Cr layer. The positions of the molecule O atoms are indicated by thin vertical lines.

with the densities of the total system (SM), and the clean surface (S) and isolated molecule (M), the latter two constrained to stay in the atomic geometry of the adsorbed system. The density difference shows how the electrons rearrange upon the adsorption. The results are presented in figures 3 and 4. The full lines indicate an increase in electron density, and the dashed line a decrease in electron density.

In figure 5 we have plotted the electron density difference $\Delta n(\mathbf{r})$ integrated in the plane parallel to the [0001] direction, which we denote the z-direction,

$$\Delta n_{1D}(z) = \int \mathrm{d}\sigma \, \Delta n(\mathbf{r}). \tag{7}$$

Two conclusions can be drawn from this plot. In both cases, only the top layer of the oxide is affected by the adsorption, whereas the lower lying layers are unaffected. Second, for *methanol*, the top panel of figure 5 shows that there is gain of electrons in the slab region, whereas for *methoxy*, the bottom panel shows a loss of electrons. To estimate the charge transfer between the adsorbates and the surface we summed over the Bader charges corresponding to the atoms of the molecule. For *methanol*, this calculation yields a loss of electron density, corresponding to an increase of positive charge of 0.02 $|e|$ compared to the gas phase molecule; for *methoxy* a similar calculation shows a gain of electron density corresponding to a reduction of positive charge of 0.41 $|e|$. This is expected: the closed-shell methanol molecule stays (almost) neutral, while there is a charge transfer to the methoxy radical with its partially empty highest occupied orbital (2e) [47].

We first comment on the electron density difference contour plots for adsorbed methanol. It is evident from figure 3 that both the surface layer Cr and O atoms are involved in the methanol–substrate interaction. Figure 3(c) shows a loss of electron density near the hydroxyl group H atom, and a build-up of electron density between the H atom and the surface O atom (O_s).

Together with the elongation of the methanol O–H bond (table 3) and the short distance between O_s and the methanol O atom (O_{ads}) of 2.57 Å (shorter than the O–O distance in ordinary ice Ih of 2.76 Å), this suggests a H–O_s contribution to the methanol–surface bonding.

Although methanol is a closed-shell molecule, the highest occupied orbital of methanol is a non-bonding ('lone-pair') orbital localized on the O atom [46], which may interact with (partially) empty surface cation states to form a (covalent) donor–acceptor bond [48]. We interpret the build-up of electron density between the O_{ads} and Cr atom (characteristic of a covalent bond) as a support for such a bonding mechanism.

The electron density difference plot for methoxy adsorbed at the α-Cr_2O_3(0001) surface (figure 4) shows a gain of electron density at the methoxy molecule in a shape distinctive of the partially filled highest occupied (2e) orbital [49], consistent with the charge transfer from the surface noted above. The induced changes in the electron density at the surface Cr atom exhibits a d_{z^2} and d_{xz}/d_{yz} character, indicating a bonding mechanism mainly involving these states and the methoxy 2e orbital.

5. Discussion and conclusions

In contrast to our previous findings [22, 23] for α-Al_2O_3(0001), the adsorption energy and structure of methanol on α-Cr_2O_3(0001) hardly changes with coverage. The preference for a full coverage of methanol or methoxy on Cr_2O_3 agrees well with the experimental findings of Badlani and Wachs [50] who found that the number of surface active sites N_s for methanol chemisorption and possible subsequent dissociation is 12.4 μmol m^{-2} at 100 °C (unspecified surface directions). A full coverage ($\Theta = 1$ ML) in our calculations corresponds to $N_s = 7.8$ μmol m^{-2}. In comparison, on Al_2O_3 Badlani and Wachs found $N_s = 5.6$ μmol m^{-2}, where we found the coverage $\Theta = 1/4$ ML (i.e., $N_s = 1.8$ μmol m^{-2}) to be most favourable [22, 23].

The adsorption sites for methanol on the two surfaces differ. Thus, although both materials are similar in atomic structure, the electronic (and magnetic) structure of the materials differs sufficiently to lead to different adsorption situations. We note that our DFT results for the structure of the methanol adsorption, figure 3, are consistent with expectations of a simple, electrostatic model analysis. There one expects the electron-rich O atom to sit close to an exposed surface cation while the H atom of the OH group points towards a surface anion. This is also expected from simple chemical (lone-pair) bonding arguments.

Whereas methanol adsorption is not dissociative on α-Al_2O_3(0001) (in the absence of co-adsorbed H atoms), our results for methanol adsorption on α-Cr_2O_3(0001) indicate that dissociation may take place to obtain the energetically preferred methoxy adsorption, at least as an intermediate product. The energy gain in adsorbing methoxy via methanol dissociation instead of adsorbing undissociated methanol is a small 0.08 eV per molecule. This fact makes it possible that methanol and methoxy will co-adsorb on α-Cr_2O_3(0001). The elongation of the hydroxyl O–H bond towards the surface O can be interpreted as the first step in such a process.

Although our results here are for the defect-free and clean α-Cr_2O_3(0001) we believe that our results will qualitatively carry over also to more realistic CCC surfaces. Thus one difference in (paint) polymer adhesion on alumina and chromia surfaces is that the dissociation of the hydroxyl groups of the polymers is more likely on chromia than on alumina, yielding different mechanisms for the binding of paint to the two surfaces.

In conclusion, we have by first-principles calculations characterized the α-Cr_2O_3(0001) surface and its adsorption of methanol and methoxy molecules at different coverages. We found strong (3.3 eV) binding of methoxy to the surface, while the methanol binding is weaker (0.8 eV). We have described the geometrical structure of the molecules and surface upon adsorption, and have analysed the changes on the electron density due to adsorption.

Acknowledgments

This work was partly carried out within *Light Metal Surface Science*, a joint project between SINTEF and NTNU, financed by The Norwegian Research Council (NFR), Hydro Aluminium, Profillakkering AS, Norsk Industrilakkering AS, Fundamus AS, Jotun Powder Coatings AS, and DuPont Powder Coating. NFR and NTNU are acknowledged for support through computing time at the Norwegian High Performance Computing Center (NOTUR). The work of ES was supported by the Swedish Research Council (VR) and the Swedish Foundation for Strategic Research (SSF) through the consortium ATOMICS.

References

[1] McDaniel M P 1985 *Adv. Catal.* **33** 47
[2] Scarano D, Spoto S, Bordigia S, Carnelli L, Ricchiardi G and Zecchina A 1994 *Langmuir* **10** 3094
[3] Mensch M W, Byrd C M and Cox D F 2003 *Catal. Today* **85** 279
[4] Curry-Hyde H E, Musch H and Baiker A 1990 *Appl. Catal.* **65** 211
[5] Miremadi B K, Singh R C, Chen Z, Roy Morrison S and Colbow K 1994 *Sensors Actuators* B **21** 1
[6] Adams R O 1983 *J. Vac. Sci. Technol.* A **1** 12
[7] Marcus P and Maurice V 2000 Passivity of metals and alloys *Corrosion and Environmental Degradation* (*Materials Science and Technology, A Comprehensive Treatment* vol 19) ed M Schütze (Weinheim: Wiley–VCH)
[8] Huppatz W, Paul M and Friedrich S 2003 Surface treatment of aluminium *Forming, Casting, Surface Treatment, Recycling and Ecology* (*Aluminium Handbook* vol 2) ed G Drossel *et al* (Düsseldorf: Aluminium)
[9] Sharrock M P 1989 *IEEE Trans. Magn.* **25** 4374
[10] Critchlow G W, Yendall K A, Bahrani D, Quinn A and Andrews F 2006 *J. Adhes. Adhesives* **26** 419
[11] Rehbein C, Harrison N M and Wander A 1996 *Phys. Rev.* B **54** 14066
[12] Rohr F, Bäumer M, Freund H-J, Mejias J A, Staemmler V, Müller S, Hammer L and Heinz K 1997 *Surf. Sci.* **372** L291
Rohr F, Bäumer M, Freund H-J, Mejias J A, Staemmler V, Müller S, Hammer L and Heinz K 1997 *Surf. Sci.* **389** 391 (erratum)
[13] Maurice V, Cadot S and Marcus P 2000 *Surf. Sci.* **458** 195
[14] Wolter K, Scarano D, Fritsch J, Kuhlenbeck H, Zecchina A and Freund H-J 2000 *Chem. Phys. Lett.* **320** 206
[15] Wang X-G and Smith J R 2003 *Phys. Rev.* B **68** 201402
[16] Rohrbach A, Hafner J and Kresse G 2004 *Phys. Rev.* B **70** 125426
[17] Bredow T 1998 *Surf. Sci.* **401** 82
[18] Henderson M and Chambers S A 2000 *Surf. Sci.* **449** 135
[19] Pykavy M, Staemmler V, Seiferth O and Freund H-J 2001 *Surf. Sci.* **479** 11
[20] Seiferth O, Wolter K, Dillmann B, Klivenyi G, Freund H-J, Scarano D and Zecchina A 1999 *Surf. Sci.* **421** 176
[21] Hemmerich I, Rohr F, Seiferth O, Dillmann B and Freund H-J 1997 *Z. Phys. Chem.* **202** 31
[22] Borck Ø and Schröder E 2003 *ATB-Metallurgie* **43** 342
[23] Borck Ø and Schröder E 2006 *J. Phys.: Condens. Matter* **18** 1
[24] The plane-wave pseudo-potential DFT code DACAPO can be downloaded from http://dcwww.fysik.dtu.dk/campos/Dacapo
[25] Vanderbilt D 1990 *Phys. Rev.* B **41** 7892
[26] Perdew J P, Chevary J A, Vosko S H, Jackson K A, Pederson M R, Singh D J and Fiolhais C 1992 *Phys. Rev.* B **46** 6671
Perdew J P, Chevary J A, Vosko S H, Jackson K A, Pederson M R, Singh D J and Fiolhais C 1993 *Phys. Rev.* B **48** 4978 (erratum)
[27] Monkhorst H J and Pack J D 1976 *Phys. Rev.* B **13** 5188
[28] Neugebauer J and Scheffler M 1992 *Phys. Rev.* B **46** 16067
[29] Bengtsson L 1999 *Phys. Rev.* B **59** 12301
[30] Press W, Flannery B, Teukolsky S A and Vetterling W T 1992 *Numerical Recipes in Fortran* 2nd edn (Cambridge: Cambridge University Press)
[31] Bader R F W 1990 *Atoms in Molecules—A Quantum Theory* (Oxford: Oxford University Press)
[32] Henkelman G, Arnaldsson A and Jónsson H 2006 *Comput. Mater. Sci.* **36** 354
[33] Wyckoff R W G 1964 *Crystal Structures* 2nd edn (New York: Interscience)

[34] Corliss L M, Hastings J M, Nathans R and Shirane G 1965 *J. Appl. Phys.* **36** 1099
[35] Finger L W and Hazen R M 1980 *J. Appl. Phys.* **51** 5362
[36] Sato Y and Akimoto A 1979 *J. Appl. Phys.* **50** 5285
[37] Chase M W 1998 *NIST-JANAF Thermochemical Tables* 4th edn (Woodbury, NY: American Institute of Physics and American Chemical Society)
[38] Ziambaras E and Schröder E 2003 *Phys. Rev.* B **68** 064112
[39] Jaffe J E, Dupuis M and Gutowski M 2004 *Phys. Rev.* B **69** 205106
[40] Kurth S, Perdew J P and Blaha P 1999 *Int. J. Quantum Chem.* **75** 889
[41] Filipi C, Singh D J and Umrigar C J 1994 *Phys. Rev.* B **50** 14947
[42] Stampfl C, Mannstadt W, Asahi R and Freeman A J 2001 *Phys. Rev.* B **63** 155106
[43] Brown P J, Forsyth J B, Lelièvre-Berna E and Tasset F 2002 *J. Phys.: Condens. Matter* **14** 1957
[44] Zimmermann R, Steiner P, Claessen R, Reinert F, Hüfner S, Blaha P and Dufek P 1999 *J. Phys.: Condens. Matter* **11** 1657
[45] Borck Ø *et al* 2006 unpublished
[46] Rolke J, Zheng Y, Brion C E, Shi Z, Wolfe S and Davidson E R 1999 *Chem. Phys.* **244** 1
[47] Jackels C F 1985 *J. Chem. Phys.* **82** 311
[48] Henrich V E and Cox P A 1994 *The Surface Science of Metal Oxides* (Cambridge: Cambridge University Press)
[49] Rodriguez J A 1992 *Surf. Sci.* **273** 385
[50] Badlani M and Wachs I E 2001 *Catal. Lett.* **75** 137